Structures and Phase Transitions of CePd$_{3+x}$Ga$_{8-x}$: New Variants of the BaHg$_{11}$ Structure Type

Melanie C. Francisco,[1] Christos D. Malliakas,[4] Robin T. Macaluso,[2] Joseph Prestigiacomo,[3] Neel Haldolaarachchige,[3] Philip W. Adams,[3] David P. Young,[3] Ying Jia,[4] Helmut Claus,[4] K.E. Gray,[4] and Mercouri G. Kanatzidis[4],*

[1]Department of Chemistry, Northwestern University, Evanston, Illinois 60208, United States

[2]Department of Chemistry and Biochemistry, University of Northern Colorado, Greeley, Colorado 80639, United States

[3]Department of Physics and Astronomy, Louisiana State University, Baton Rouge, Louisiana 70803, United States

[4]Materials Science Division, Argonne National Laboratory, Argonne, Illinois 60439, United States

Ⓢ *Supporting Information*
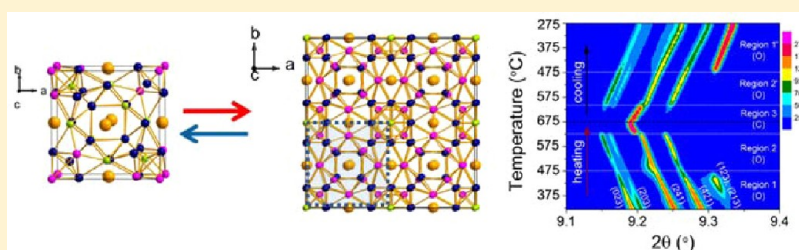
ABSTRACT: New distorted variants of the cubic BaHg$_{11}$ structure type have been synthesized in Ga flux. Multiple phases of CePd$_{3+x}$Ga$_{8-x}$, which include an orthorhombic *Pmmn* structure ($x = 3.21(2)$), a rhombohedral $R\overline{3}m$ structure ($x = 3.13(4)$), and a cubic $Fm\overline{3}m$ superstructure ($x = 2.69(6)$), form preferentially depending on reaction cooling rate and isolation temperature. Differential thermal analysis and *in situ* temperature-dependent powder X-ray diffraction patterns show a reversible phase transition at approximately 640 °C between the low temperature orthorhombic and rhombohedral structures and the high temperature cubic superstructure. Single crystal X-ray diffraction experiments indicate that the general structure of BaHg$_{11}$, including the intersecting planes of a kagomé-type arrangement of Ce atoms, is only slightly distorted in the low temperature phases. A combination of Kondo, crystal electric field, and magnetic frustration effects may be present, resulting in low temperature anomalies in magnetic susceptibility, electrical resistivity, and heat capacity measurements. In addition to CePd$_{3+x}$Ga$_{8-x}$, the rare earth analogues REPd$_{3+x}$Ga$_{8-x}$, RE = La, Nd, Sm, Tm, and Yb, were successfully synthesized and also crystallize in one of the lower symmetry space groups.

■ INTRODUCTION

Intermetallic compounds show a wealth of novel bonding patterns and physical properties,[1−6] which motivates chemists to discover new phases. Traditional solid-state synthesis techniques for intermetallics rely heavily on high temperature melting methods such as arc melting and radio frequency (RF) induction. Although these techniques remain valuable synthetic tools, an incredible number of new compounds can be accessed through utilization of lower temperature methods if diffusion rates can be enhanced and better controlled. The molten metal flux method has proven to be a fruitful synthetic technique for the discovery of new compounds and single crystals.[2,7−13] Metals are brought into solution at substantially lower temperatures than melting methods and reactions can be conducted in simple resistance furnaces where critical reaction parameters can be varied easily. Most significantly, reaction time and heating and cooling rates can be systematically changed in ways that may lead to formation of different compounds for the same set of elements and starting ratios. For

example, synthesis of LnNi$_{1-x}$Ga$_4$ (Ln = Tb−Er) in Ga flux contains a mixture of α-LnNiGa$_4$ and β-LnNi$_{1−x}$Ga$_4$ that can be tuned to favor the β-LnNi$_{1−x}$Ga$_4$ form by utilizing a two-step cooling sequence.[14] Similarly, β-RENiGe$_2$ (RE = Er, Dy) can be isolated at 850 °C in indium flux while only the α-phase is formed through arc melting, with or without indium.[12] Creation of new compounds can result by taking advantage of both thermodynamic and kinetic relationships between reactants and products in fluxes.

Previous studies in the Ce−Pd−Ga system have found intriguing low temperature magnetic structures in the ternary compounds CePdGa$_6$ and Ce$_2$PdGa$_{12}$, such as heavy fermion and metamagnetic behavior, respectively.[15,16] Kondo behavior was observed in CePdGa$_3$, along with anomalous transport properties.[17] In the Ce−Pd−Al system, the heavy fermion compound CePdAl contains geometrically frustrated Ce atoms

in a distorted kagomé arrangement, in coexistence with ordered Ce atoms.[18,19] As a result, a complex magnetic structure forms at low temperature in which spins order antiferromagnetically by an incommensurate magnetic propagation vector.[20] Similarly, the $BaHg_{11}$ structure type[21] features intersecting kagomé sublattices formed by the Ba atoms (Figure 1) and,
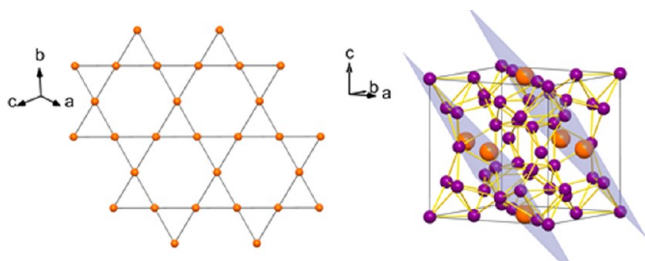

Figure 1. A kagomé net composed of corner-sharing triangles (left). The Ba-containing kagomé sublattices of the cubic $BaHg_{11}$ structure, viewed down $[1\,{-}2\,0]$, lie within the $\{111\}$ planes (highlighted, right).

thus, Ce analogues could give rise to interesting magnetic properties such as magnetic frustration between magnetic ions occupying the Ba sites with antiferromagnetic spin interactions in a triangular geometry. Several binary compounds exist in the $BaHg_{11}$ structure type, as well as a catalog of ternary and quaternary variations, including an astonishing variety of stuffed variants in which an extra element occupies cubic vacancies in the structure.[22−33] Several reported compounds show interesting low temperature properties, such as superconductivity in KHg_{11} and $RbHg_{11}$[24] and antiferromagnetic ordering in $CeCd_{11}$ and $PrCd_{11}$.[34] These findings make $CePd_{3+x}Ga_{8-x}$ a promising compound to study its physical properties at low temperature.

The compound $CePd_{3+x}Ga_{8-x}$ was successfully synthesized by the molten metal flux technique, with Ga flux, after optimization of reaction conditions. The new phase, however, did not crystallize with cubic $Pm\overline{3}m$ symmetry as expected for $BaHg_{11}$ structures. Variation of the heating treatment produced a total of three phases of different symmetry: orthorhombic $Pmmn$ (O-$CePd_{3.21(2)}Ga_{7.79(2)}$), rhombohedral $R\overline{3}m$ (R-$CePd_{3.13(4)}Ga_{7.87(4)}$), and cubic $Fm\overline{3}m$ (C-$CePd_{2.69(6)}Ga_{8.31(6)}$). The $CePd_{3+x}Ga_{8-x}$ phases exhibit unique polymorphic transitions between high- and low-temperature phases in that two low-temperature phases of $CePd_{3+x}Ga_{8-x}$ are accessible from the same high-temperature phase. The structural complexity and sensitivity to small perturbations to the system make $CePd_{3+x}Ga_{8-x}$ an interesting compound in which to examine the determinants of structural stability in intermetallics in general.

This study reveals the intricacies in both structure and low temperature properties of the $REPd_{3+x}Ga_{8-x}$ family of compounds, where RE is a rare earth element. *In situ* high-resolution X-ray diffraction experiments and thermal analysis were conducted to study structural relationships and transformations between O-$CePd_{3.21}Ga_{7.79}$ and C-$CePd_{2.68}Ga_{8.31}$. A rearranged and distinct orthorhombic phase formed approximately 200 °C before conversion to the cubic phase, showing a unique multistep phase transformation from O- to C-$CePd_{3-x}Ga_{8-x}$. Interesting ground states were also discovered in the low-temperature physical properties. Interplay of Kondo behavior and other anomalous behavior, possibly magnetic frustration, were found in magnetic susceptibility, electrical resistivity, and heat capacity measurements.

■ EXPERIMENTAL METHODS

Synthesis. An amount of 0.75 mmol Ce (0.105 g, powder filed from Ce ingot, Atlantic Equipment Engineers, 99.9%), 3 mmol Pd (0.319 g; −200 mesh, Alfa Aesar, 99.95% or −325 mesh Pd, Johnson Mahony, 99.95%) and 11.25 mmol Ga (0.784 g, crushed pieces from Ga teardrops, Plasmaterials, 99.999%) were added to an alumina crucible and inserted into a fused silica tube under nitrogen atmosphere. A mesh filter was placed on top of the crucible for centrifugation after reaction and the tube was flame-sealed under vacuum at $<1 \times 10^{-3}$ mbar. Reactions were placed upright in a box furnace and the following temperature programs were applied to isolate the various forms:

O-$CePd_{3.21}Ga_{7.79}$: Heated to 1000 °C (65 °C/h), soaked for 5 h, cooled to 600 °C (5.83 °C/h), soaked for 12 h, and quenched in cold water. The tube was reheated to 300 °C then quickly inverted and centrifuged at 2800 rpm to remove excess flux. Alternatively, the reaction can be cooled from 1000 to 860 °C (5.83°/h), soaked for 60 h, slowly cooled to 600 °C (10.83 °C/h) then quickly cooled to 300 °C (100°/h) and centrifuged.

R-$CePd_{3.17}Ga_{7.83}$: Heated to 1000 °C (65 °C/h), soaked for 5 h, cooled to 860 °C (5.83 °C/h), soaked for 60 h, and cooled to 300 °C (75 °C/h). At 300 °C, the tube was quickly inverted and centrifuged at 2800 rpm to remove excess flux. Alternatively, R-$CePd_{3.13}Ga_{7.87}$ could be isolated by heating to 1100 °C (65 °C/h), soaking for 2 h, and cooling to 300 °C (60 °C/h) and centrifuging.

C-$CePd_{2.69}Ga_{8.31}$: Heated to 1000 °C (58 °C/h), cooled to 675 °C (10 °C/h), soaked for 22 h, and then quenched into a cold water bath. The reaction was reheated to 200 °C and centrifuged at 2800 rpm for ~20 s to remove excess flux.

Hand-picked silver-colored, faceted cubic crystals were immersed in a 3 M solution of iodine (I_2) in *N,N*-dimethylformamide (DMF) and soaked for up to 1 h to remove Ga flux from the surface. To clean the entire reaction product, samples were soaked from 4 h to overnight depending on the efficacy of the centrifuge process. The samples were washed with DMF and deionized water then rinsed with acetone and dried in air. The major side product was crystalline $PdGa_5$, which contributed about 20% of the phases present with 80% $CePd_{3+x}Ga_{8-x}$, as identified by powder X-ray diffraction. In most reactions, crystalline Ce_2PdGa_{12} was present as a minor phase, and in some cases a few crystals of $CePd_2Ga_2$, $CePdGa_6$, and Pd_3Ga_7 were found, which exemplifies the highly dense phase space for this set of reaction conditions.

Energy-Dispersive Spectroscopy. Semiquantitative elemental analysis was performed on a Hitachi SEM-3400 equipped with an Oxford Instruments detector. Single crystals were analyzed under 20 keV accelerating voltage and 45−60 s accumulation time. Multiple spots on several R-$CePd_{3.13}Ga_{7.87}$ and O-$CePd_{3.21}Ga_{7.79}$ crystals were analyzed with an average composition in close agreement with results from single crystal diffraction structure refinement: $Ce_{1.0(1)}Pd_{3.4(1)}Ga_{7.5(1)}$.

Powder X-ray Diffraction. Ground powder samples were analyzed on a PANanalytical X'Pert diffractometer equipped with Cu(Kα) radiation (λ= 1.540598 Å). Phase identification was carried out by comparison with simulated powder patterns calculated from single crystal structure refinements.

Single Crystal X-ray Diffraction. Room temperature single crystal data were collected on a STOE 2T image plate diffractometer with Mo(Kα) radiation (λ = 0.71073 Å) using the X-Area suite of programs provided by STOE.[35] Data collection covered a full sphere of reciprocal space. A numerical absorption correction was applied using the program X-Red on an optimized shape obtained with the aid of FaceIt and X-Shape software.[35] The structures were solved with direct methods and refined with the SHELXTL software package.[36] Anisotropic atomic displacement parameters were refined for all atomic positions. Mixed Pd/Ga sites were tested by independently refining each Pd and Ga site as a mixed site with the site occupation factor constrained to unity. Atomic coordinates and displacement parameters for each mixed site were constrained to be identical with the EXYZ and EADP commands, respectively. A pseudoracemic twin

law of (0 1 0) (1 0 0) (0 0 −1) and a refined BASF term were used for R-CePd$_{3.13}$Ga$_{7.87}$ and O-CePd$_{3.21}$Ga$_{7.79}$ structures. Atomic positions and anisotropic displacement parameters are included in the Supporting Information.

High-Resolution Variable-Temperature X-ray Powder Diffraction. High-resolution synchrotron powder X-ray diffraction data were collected on beamline 11-BM[37,38] at the Advanced Photon Source (APS) at Argonne National Laboratory using an average wavelength of 0.41397 Å. A baseline diffraction pattern was collected at 295 K (λ = 0.41361 Å) prior to the heating experiment. The discrete detectors, covering an angular range from −6 to 16° 2θ, were scanned over a 34° 2θ range beginning at −6° 2θ. Data points were collected every 0.001° 2θ with a scan speed of 0.01°/s. Rietveld refinement results on the orthorhombic phase are included in the Supporting Information. For the heating experiment, the detectors were scanned over a 10° range beginning at −4.5° in 2θ. Data points were collected every 0.002° with a scan speed of 0.03°/s. Samples were vacuum sealed in 0.3 mm diameter quartz capillaries to prevent oxidation. During collection, samples were spun at 5400 rpm and heated and cooled *in situ* from 300 to 675 °C at a continuous ±5°/min temperature ramp using a Cyberstar hot gas blower accessory. This resulted in an approximately 20° temperature smear for each scan.

Magnetic Susceptibility. Magnetic susceptibility measurements were performed on a Quantum Design MPMS SQUID or PPMS magnetometer. Several single crystals (10−20 mg) were randomly aligned inside kapton tape or a gelatin capsule with a small amount of quartz wool, to prevent sample movement, and then secured in a clear plastic straw. Magnetization was recorded in the temperature range 2−300 K in an applied field of 1 T, which is below the saturation field determined by preliminary magnetization versus field sweeps at 5 K. Data were corrected for core diamagnetism using Pascal's constants.[39]

The antiferromagnetic transition temperature, T_N, was determined with a noncommercial low-field SQUID magnetometer.[40] The samples were cooled in zero field to a temperature below T_N. Then a low field was applied and the magnetization was recorded during warming. The earth's magnetic field was shielded by an *m*-metal shield yielding a remnant magnetic field of less than 10 mGauss. Magnetic fields up to 50 G were obtained with a Cu solenoid.

Electrical Resistivity. Four gold wires were attached in a linear four-probe configuration to a single crystal sample of O-CePd$_{3+x}$Ga$_{8−x}$ using silver epoxy cured at approximately 130 °C for 20 min. After cooling under zero field, resistance data were collected on warming under zero applied field and 3 T with a DC current of 1 mA.

Heat Capacity. Heat capacity versus temperature measurements were performed using a Quantum Design PPMS equipped with a Helium-3 refrigerator option. Each run was performed starting from the lowest temperature to the highest and applied magnetic field data were taken following a zero field-cooled protocol. Thermal contact between the sample and the measurement platform was maintained by applying a small amount of Apiezon N grease. The heat capacity of the grease and platform was measured prior to mounting the sample in order to subtract their contribution to the total heat capacity. The step size of this measurement was sufficiently small as to eliminate the potential for false peaks that may appear as artifacts introduced by the interpolation scheme of the automatic background subtraction used by the heat capacity software. A temperature rise of 2% of the sample temperature was employed for each measurement. This value is large enough to perform accurate fitting of the relaxation in temperature after applying heat to the sample, yet small enough as to not overshoot the temperature region where transitions reside and wash out any peak features in the data. The criterion for sample temperature stability between measurements was established so that it may not vary more than 0.3% of the subsequently applied temperature rise. This reduces scatter in the data as was verified by performing three repetitions per measurement.

■ RESULTS AND DISCUSSION

Synthesis, Structure, and Interconversions.
All compounds were synthesized using the molten metal flux technique

in excess Ga.[2] Results were sensitive to changes in the physical form of the starting reagents and to the reaction scale. Several Ce−Pd−Ga ternary compounds are known and were found as minor to major products in different reactions; these included Ce$_2$PdGa$_{12}$, CePdGa$_6$, and CePd$_2$Ga$_2$. Nearly phase-pure Ce$_2$PdGa$_{12}$ resulted from a 1Ce:3Pd:15Ga molar ratio reaction using Pd foil. Since CePd$_3$Ga$_8$ is the most Pd-rich system in the set of Ce−Pd−Ga compounds, a more Pd-rich molar ratio 1Ce:4Pd:15Pd was subsequently employed. Synthesis on a 0.75 mmol reaction scale, using a fine mesh Pd powder, was successful in producing CePd$_{3+x}$Ga$_{8−x}$ in high yield. An SEM image of a typical faceted cubic single crystal of CePd$_{3+x}$Ga$_{8−x}$ resulting from such reactions is shown in Figure 2. The best
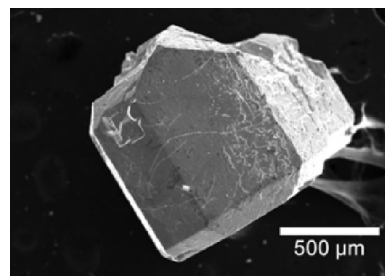

Figure 2. SEM image of a typical single crystal of CePd$_{3+x}$Ga$_{8−x}$ grown from Ga flux.

crystal quality, in terms of well-defined faces and minimum surface crevices, agglomerated crystals, and inclusions, was found using −325-mesh Pd powder. Quality was noticeably reduced when using the slightly larger −200-mesh Pd particle size and very poor using −60-mesh particle size. Poor crystal quality was accompanied by a higher fraction of other Ce−Pd−Ga side products, as well as difficulty in controlling the formation of rhombohedral versus orthorhombic phases. Attempts to synthesize the pure CePd$_{3+x}$Ga$_{8−x}$ phase by direct combination melting techniques were unsuccessful.

The strong dependence on the form of the starting materials suggests that kinetic processes affect product formation on heating as well as on cooling. Solution dynamics are in stark contrast to the dynamics of high temperature syntheses in which the high energies available limit discoveries to thermodynamic products. In solution, where the diffusion process is slower, formation of products is likely to depend on intermediates or clusters, and how readily they can form at certain temperatures. Initial reagents in powder form will result in a homogeneous dispersion of reactants much more quickly than larger chunks of metal, which may not have time to diffuse sufficiently into solution before reactions begin and this may affect what products form at the end. We suspect one of the key intermediate steps in the formation of CePd$_{3+x}$Ga$_{8−x}$ occurs on heating and is hindered when Pd dispersion is slow.

The reaction kinetics on cooling from high temperature controls the formation of the distorted phases of CePd$_{3+x}$Ga$_{8−x}$. Quickly cooling from 860 °C (>60°/h) produced crystals with $R\bar{3}m$ rhombohedral symmetry, as previously reported.[41] Slowly cooling to 600 °C (<11°/h) and then quickly cooling to 300 °C (100°/h) led to crystals with $Pmmn$ orthorhombic symmetry. In some cases, a few crystals of orthorhombic and rhombohedral phases were found as impurities (e.g., orthorhombic crystals found in a fast cooling reaction); however, powder X-ray diffraction showed that the majority of phases formed according to the described cooling procedures. A slow

cooling profile from 860 °C continuously down to 300 °C (<12°/h) produced highly disordered and twinned crystals. Powder X-ray diffraction patterns of the slow-cooled product imply orthorhombic symmetry; however, a satisfactory single crystal X-ray structure refinement could not be obtained due to poor crystal quality. A third, high symmetry $Fm\bar{3}m$ cubic phase of $CePd_{3+x}Ga_{8-x}$ could be isolated from reactions in which the tubes were quenched from 675 °C into a cold water bath (∼20 °C). These phase relationships are summarized in Figure 3.
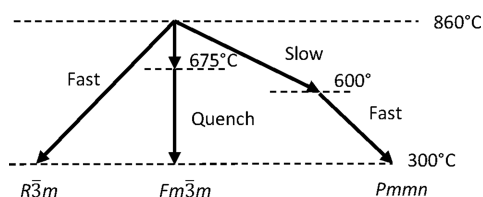

Figure 3. Summary of $CePd_{3+x}Ga_{8-x}$ phases isolated from Ga flux. The high temperature cubic phase can be isolated by quenching from 675 °C. If cooled less than 675 °C, the cubic phase distorts to rhombohedral or orthorhombic symmetry.

Crystallographic refinement information from single crystal X-ray diffraction data is given in Table 1. The electron difference map was checked carefully for signs of missed electron density inside the cubic subunits in light of the prevalence of stuffed positions in the aluminides and in $K_3Mg_{20}In_{14}$,[22,25,28,29] We conclude that the $CePd_{3+x}Ga_{8-x}$ compounds are unstuffed variants of the $BaHg_{11}$ structure. Atomic positions and anisotropic atomic displacement parameters can be found in Supporting Information. Empirical formulas for the rhombohedral and orthorhombic phases, as well as the high symmetry cubic phase, refined as the following: R-$CePd_{3.13(4)}Ga_{7.87(4)}$, O-$CePd_{3.2(2)}Ga_{7.79(2)}$, and C-$CePd_{2.69(6)}Ga_{8.31(6)}$.

The synthesized compounds did not crystallize in the ideal $BaHg_{11}$-type structure with cubic $Pm\bar{3}m$ symmetry, but rather in distorted variants of the parent structure. The cubic $BaHg_{11}$ structure is made up of three main structural units, as highlighted in Figure 4: Hg_{12} cuboctahedra formed around a Hg atom, empty Hg_8 cubes, and $Ba@Hg_{20}$ polyhedra. Variants of the $BaHg_{11}$ structure can include elemental substitutions on one Ba position and four unique Hg positions. A view of the

Table 1. Single Crystal X-ray Diffraction Structure Refinement Summary for $CePd_{3+x}Ga_{8-x}$ Phases[a]

empirical formula	$CePd_{3.13(4)}Ga_{7.87(4)}$	$CePd_{3.21(2)}Ga_{7.79(2)}$	$CePd_{2.9(1)}Ga_{8.1(1)}$	$CePd_{2.69(6)}Ga_{8.31(6)}$
cooling rate (°C/h)	75	5.83	n/a	10
isolation temp (°C)	300	600	675	675
formula weight (g/mol)	1021.91	1024.85	1012.00	1005.76
temperature (K)	293(2)	293(2)	293(2)	293(2)
wavelength (Å)	0.71073	0.71073	0.71073	0.71073
crystal system	rhombohedral	orthorhombic	cubic	cubic
space group	$R\bar{3}m$	$Pmmn$	$Pm\bar{3}m$	$Fm\bar{3}m$
crystal color			silver	
unit cell dimensions (Å)	$a = 11.994(2)$	$a = 11.8617(6)$	$a = 8.4643(9)$	$a = 16.8984(8)$
	$b = 11.994(2)$	$b = 11.9511(5)$	$b = 8.4643(9)$	$b = 16.8984(8)$
	$c = 14.639(3)$	$c = 8.5065(3)$	$c = 8.4643(9)$	$c = 16.8984(8)$
volume (Å³)	1823.8(6)	1205.88(9)	606.42(11)	4825.4(4)
Z	9	6	3	24
Density (g/cm³)	8.334	8.403	8.355	8.400
Absorption coefficient (mm⁻¹)	37.988	38.302	38.083	38.287
$F(000)$	3996	2664	1332	10656
Crystal size (mm³)	$0.08 \times 0.08 \times 0.10$	$0.07 \times 0.07 \times 0.15$	$0.03 \times 0.06 \times 0.08$	$0.05 \times 0.13 \times 0.20$
Theta range for data collection (°)	4.16 to 34.82°	3.82 to 36.44°	3.40 to 34.50°	4.00 to 34.79°
Index ranges	$-19 \leq h \leq 18$,	$-19 \leq h \leq 19$,	$-13 \leq h \leq 13$,	$-27 \leq h \leq 27$,
	$-19 \leq k \leq 19$,	$-19 \leq k \leq 19$,	$-13 \leq k \leq 13$,	$-22 \leq k \leq 27$,
	$-19 \leq l \leq 23$	$-14 \leq l \leq 12$	$-11 \leq l \leq 13$	$-26 \leq l \leq 27$
reflections collected	8871	19870	8546	11452
independent reflections	979 [$R(int) = 0.0505$]	3160 [$R(int) = 0.0508$]	310 [$R(int) = 0.0518$]	581 [$R(int) = 0.0413$]
completeness to theta (%)	98.80 to 34.82°	99.50 to 36.44°	99.00 to 34.50°	99.30 to 34.79°
absorption correction			integration	
max and min transmission	0.3845 and 0.1976	0.1450 and 0.0508	0.3630 and 0.1173	0.4143 and 0.0621
refinement method			full-matrix least-squares on F^2	
data/restraints/parameters	979/0/42	3160/0/102	310/0/21	581/0/29
twin fraction [010][100][00−1]	0.0021	0.0170	N/A	N/A
goodness-of-fit on F^2	1.191	1.095	1.402	2.684
final R indices [$I > 2\sigma(I)$]	R1 = 0.0376,	R1 = 0.0417,	R1 = 0.0352,	R1 = 0.0397,
	wR2 = 0.0672	wR2 = 0.0942	wR2 = 0.0584	wR2 = 0.0706
R indices (all data)	R1 = 0.0441,	R1 = 0.0501,	R1 = 0.0386,	R1 = 0.0430,
	wR2 = 0.0692	wR2 = 0.0988	wR2 = 0.0592	wR2 = 0.0718
extinction coefficient	0.00025(3)	0.00429(12)	0.00205(19)	0.000048(5)
largest diff. peak and hole (e Å⁻³)	2.513 and −2.035	2.541 and −2.739	2.215 and −2.710	2.991 and −1.566

[a]Annealed crystals were analyzed for R-$CePd_{3.13}Ga_{7.87}$ (500°C) and $Pm\bar{3}m$ $CePd_{2.9(1)}Ga_{8.1(1)}$ (675°C). wR2 = { Σ [$w(F_o^2 - F_c^2)^2$]/Σ [$w(F_o^2)^2$] }$^{1/2}$; R1 = Σ | $|F_o| - |F_c|$ |/Σ $|F_o|$ GoF = S = { Σ [$w(F_o^2 - F_c^2)^2$]/$(n-p)$ }$^{1/2}$.
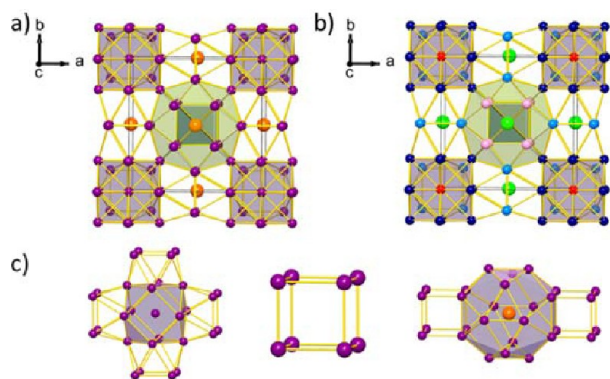
Figure 4. Unit cell of the parent structure $BaHg_{11}$: (a) unit cell viewed down [001]-direction with main structural units shaded (orange atoms are Ba, purple atoms are Hg): (b) unit cell differentiating the five Wyckoff positions; (c) isolated structural units (left to right) Hg-centered cuboctohedron, Hg_8 cube, and $Ba@Hg_{20}$ polyhedron.

unit cell, with Wyckoff positions differentiated by color, is given in Figure 4b. The Ba atoms form intersecting kagomé sublattices perpendicular to {111} planes (Figure 1).

At high temperature, $CePd_{3+x}Ga_{8-x}$ adopts an 8-fold cubic supercell with $a = 16.8984(8)$ Å and $Fm\bar{3}m$ symmetry. Supercell reflections have been observed in X-ray diffraction patterns of the quaternary analogue $Ca_3Au_{6.8}Al_{26}Ti$;[25] however,

because of a lower degree of long-range order, the structural model of the aluminide could only be refined as an average subcell structure with cubic $Pm\bar{3}m$ symmetry ($a = 8.6631(5)$ Å). The high temperature C-$CePd_{3+x}Ga_{8-x}$ phase is thus the first observation of the fully ordered supercell structure. One notable feature is that the Pd atom at the center of the cuboctahedron is surrounded solely by 12 Ga atoms and no Pd atoms. In addition, mixed Pd/Ga and Ga sites occupy alternate positions within the cubic structural unit. A comparison of structural units between the parent $BaHg_{11}$ structure and phases synthesized in this work is shown in Table 2.

Upon further cooling of the Ga flux reaction below 675 °C, cubic symmetry is lost and R-$CePd_{3.13}Ga_{7.87}$ and O-$CePd_{3.21}Ga_{7.79}$ phases form. Presumably two pathways exist from the cubic form that lead to lower symmetry forms in which both Pd/Ga site distribution and structure differ. The R-$CePd_{3.13}Ga_{7.87}$ form is pseudocubic with primitive cell dimensions $a = b = c = 8.4714(8)$ Å and $\alpha = \beta = \gamma = 90.134(8)°$ ($a = 11.994(2)$, $b = 11.994(2)$, $c = 14.639(3)$ Å and $\alpha = \beta = 90°$, $\gamma = 120°$ in standard hexagonal setting). Single crystals typically contained a high twin fraction of more than 20%, which could be reduced to less than 1% by annealing, as discussed later. A view of the cubic structural unit in annealed R-$CePd_{3.13}Ga_{7.87}$ shows that Pd and Ga are crystallographically ordered and that the Pd atoms reside along the body diagonal corners of the cube-like unit.

Table 2. Comparison of the Unit Cell and Structural Units for the Forms of $CePd_{3+x}Ga_{8-x}$ Isolated in This Study[a]

Phase	Unit Cell	Structural Units		
		Cube	Cuboctahedron	Polyhedron
Parent $Pm\bar{3}m$ ($BaHg_{11}$)				
Rhombohedral $R\bar{3}m$ (annealed)				
Orthorhombic $Pmmn$				
Cubic superstructure $Fm\bar{3}m$				
Cubic subcell $Pm\bar{3}m$				

[a]The cubic $Pm\bar{3}m$ subcell was isolated by annealing an orthorhombic $CePd_{3+x}Ga_{8-x}$ single crystal. Atom colors are as follows: Ce-gold, Pd-green, Ga-blue, mixed Pd/Ga-magenta. The structure of the parent compound $BaHg_{11}$ is also provided as a reference (Ba-orange, Hg-purple).

O-CePd$_{3.21}$Ga$_{7.79}$ is related to the cubic parent structure by $a_{ortho} \approx b_{ortho} \approx \sqrt{2}a_{cubic}$ and $c_{ortho} \approx a_{cubic}$. In a perfect cubic cell, these approximate relations would be equal. *O*-CePd$_{3.21}$Ga$_{7.79}$ crystallizes in the space group *Pmmn* with $a = 11.8617(6)$ Å, $b = 11.9511(5)$ Å, and $c = 8.5065(3)$ Å. As with *R*-CePd$_{3.13}$Ga$_{7.87}$ crystals, the *O*-CePd$_{3.21}$Ga$_{7.79}$ crystals also contained twin domains, although in much smaller fractions of about 2%. The structure is distorted significantly from the cubic BaHg$_{11}$ parent structure, although it shows some resemblance to the ordered *C*-CePd$_{2.69}$Ga$_{8.31}$ superstructure. This can be seen most clearly in the heavily distorted angles of the cube-like structural unit (Ga−Pd−Ga angles of 76.272(2)°, 83.311(7)°, and Ga−Ga−Ga angles of 78.989(4)° in *O*-CePd$_{3.21}$Ga$_{7.79}$). This may be due to the geometric constraints of having four short Pd−Ga bonds (d(Pd−Ga) = 2.62−2.64 Å, d(Ga−Ga) = 2.71−2.72 Å) on only one face of the cube-like unit in *O*-CePd$_{3.21}$Ga$_{7.79}$ versus two on every face in *R*-CePd$_{3.13}$Ga$_{7.87}$.

X-ray crystal structure models that were difficult to refine and could not be improved with annealing treatments, namely those isolated by continuous slow cooling of the reaction mixture down to 300 °C, had nearly identical a and b cell parameters in an orthorhombic setting: $a \approx 11.95$ Å, $b \approx 11.99$ Å, $c \approx 8.48$ Å ($b − a \approx 0.04$ Å). This is in contrast to *O*-CePd$_{3.21}$Ga$_{7.79}$ crystals isolated by essentially quenching from 600 °C and for which the X-ray crystal structure models refined well: $a \approx 11.86$ Å, $b \approx 11.95$ Å, $c \approx 8.50$ Å ($b − a \approx 0.09$ Å). This difference in cell parameters indicates that the crystals slow cooled down to 300 °C undergo further transformation below 600 °C and may contain more severe or complex twinning.

The bond distances between atoms in the various phases are similar as shown in Table 3. Cut-off bond distances are 3.3 Å for Pd−Ga pairs. Curiously, the longest distances are, on average, found in the rhombohedral phase and not the higher temperature orthorhombic phase. This implies that other factors play a greater role in stability than closest packing. The greatest range of bond distances for each atomic pair is found, as expected, in the more heavily distorted *O*-CePd$_{3.21}$Ga$_{7.79}$. An interesting detail is the formation of Ce−Pd and mixed Pd/Ga−Pd bonds in the lower symmetry phases that are not present in *C*-CePd$_{2.69}$Ga$_{8.31}$. These contacts may be necessary for stability at lower temperatures. The nearest Ce−Ce distances, which are relevant to magnetic Ce interactions in the kagomé sublattices, are quite similar between phases with an average distance of 5.98 ± 0.02 Å. These Ce−Ce distances are rather long compared to other Ce-containing intermetallic compounds such as CePd$_2$Al$_3$ (4.216 Å),[42] hexagonal CePdAl (3.743 Å),[43,44] and CePdGa$_6$ (4.350 Å).[16]

The ordered *C*-CePd$_{2.69}$Ga$_{8.31}$ superstructure is first to form in solution, as evidenced by quenching the compound from 675 °C. As the temperature decreases, *C*-CePd$_{2.69}$Ga$_{8.31}$ distorts to lower symmetry forms. This is supported by the fact that both low symmetry phases contain significant twin domains, an expected consequence when breaking higher symmetry. Because the compounds are in solution, bonds in *C*-CePd$_{2.69}$Ga$_{8.31}$ can break and reform and elements can continue to exchange with others in solution to form a more stable structure. Furthermore, composition may play a role in this gradual instability as *C*-CePd$_{2.69}$Ga$_{8.31}$ contains a greater Ga:Pd ratio than the structures at lower temperature.

Crystal Structures by Phase Transformations. To explore kinetic and thermodynamic products, ground crystals of *R*-CePd$_{3.13}$Ga$_{7.87}$ and *O*-CePd$_{3.21}$Ga$_{7.79}$ phases were annealed for 5 days at 500 °C. As a result, *O*-CePd$_{3.21}$Ga$_{7.79}$ converted to

Table 3. Interatomic Distances (Å) with Estimated Deviation in Parentheses for Atom Pairs in the Crystal Structural Units of CePd$_{3+x}$Ga$_{8-x}$

		atom 1	atom 2	multiplier	distance (Å)
			R-CePd$_{3.13}$Ga$_{7.87}$		
cube		Pd3	Ga1	6x	2.6095(10)
		Ga1	Ga1	6x	2.7389(10)
cuboctahedra		Pd4|Ga5	Ga2|Pd1	6x	2.7690(8)
			Ga4	6x	2.8474(10)
Ce polyhedra		Ce	Ga4	2x	3.1496(10)
			Pd2	4x	3.1671(5)
			Ga2|Pd1	2x	3.2183(8)
			Ga3	4x	3.2728(7)
			Ga1	4x	3.4077(7)
			Pd3	2x	3.4627(6)
			Ga1	2x	3.5702(10)
			O-CePd$_{3.21}$Ga$_{7.79}$		
cube		Pd3	Ga8	4x	2.5951(9)
			Ga4	2x	2.6221(13)
		Ga7	Ga4	4x	2.7203(13)
			Ga8	2x	2.7321(17)
cuboctahedra		Pd5	Ga5	2x	2.7278(12)
			Ga2	4x	2.7778(13)
			Ga3|Pd2	4x	2.8211(13)
			Ga9	2x	2.8269(12)
Ce polyhedra	1	Ce1	Pd4	2x	3.1333(3)
			Ga2	2x	3.1720(8)
			Pd1	2x	3.1774(5)
			Ga3|Pd2	2x	3.2003(8)
			Ga6	2x	3.2621(4)
			Ga1	2x	3.2715(8)
			Ga4	2x	3.4191(6)
			Pd3	2x	3.4229(4)
			Ga7	2x	3.4601(6)
			Ga8	2x	3.4972(6)
	2	Ce2	Ga9	2x	3.1550(12)
			Ga1	4x	3.1861(9)
			Ga5	2x	3.2046(12)
			Pd1	4x	3.2133(6)
			Ga7	2x	3.3997(14)
			Ga8	2x	3.4368(14)
			Ga4	2x	3.5271(13)
			Pd3	2x	3.5308(10)
			C-CePd$_{2.69}$Ga$_{8.31}$		
cube		Ga4|Pd2	Ga5	12x	2.6707(16)
cuboctahedra	1	Pd4	Ga3	12x	2.7729(9)
	2	Pd3	Ga2	12x	2.7070(9)
Ce polyhedra		Ce	Ga2	2x	3.1775(9)
			Ga1|Pd1	8x	3.2011(8)
			Ga3	2x	3.2016(9)
			Ga4|Pd2	4x	3.4495(9)
			Ga5	4x	3.4636(14)

higher symmetry, while R-CePd$_{3.13}$Ga$_{7.87}$ remained crystallized in the $R\overline{3}m$ space group. Despite a faster cooling rate from high temperature, R-CePd$_{3.13}$Ga$_{7.87}$ is the more stable product at 500 °C. The same annealing treatment on single crystals of R-CePd$_{3.13}$Ga$_{7.87}$ showed improved crystallinity, or reduced twinning, and a new distribution of Pd and Ga atoms.

An annealing treatment on a single crystal O-CePd$_{3.21}$Ga$_{7.79}$ at elevated temperature, 675 °C, for 2 days followed by quenching in cold water caused conversion to cubic symmetry. Supercell reflections were clearly visible in the single-crystal X-ray diffraction pattern; however, as in previous studies, crystals lacked sufficient long-range order to allow a satisfactory structure refinement.[29] An average structure could be refined in the $Pm\overline{3}m$ BaHg$_{11}$-type subcell to give the composition CePd$_{2.9(1)}$Ga$_{8.1(1)}$, similar to that refined for the quenched $Fm\overline{3}m$ structure. In lieu of long-range order, positional disorder and mixed occupancy models were applied within the cubic structural unit, as shown in Table 2. Presumably, a more extended annealing time on the orthorhombic phase would increase long-range order and allow refinement of the $Fm\overline{3}m$ superstructure.

A similar annealing experiment was performed on R-CePd$_{3.13}$Ga$_{7.87}$ single crystals at 675 °C for 5 days. This treatment caused conversion to cubic symmetry, again with supercell reflections. In this case, the structure could be refined in the 8-fold $Fm\overline{3}m$ superstructure with identical sites of Pd/Ga mixed occupancy as those found in the crystal quenched from solution, with a slightly lower refined Pd:Ga ratio. This further supports that only one high temperature cubic phase exists at 675 °C from which lower symmetry phases are formed.

Orthorhombic to High Symmetry Phase Transition. Differential thermal analysis (DTA) was performed on both powder and single crystal samples of O-CePd$_{3.21}$Ga$_{7.79}$ to probe the transformation to C-CePd$_{2.69}$Ga$_{8.31}$. The DTA plot on the single crystal sample is shown in Figure 5. A reversible
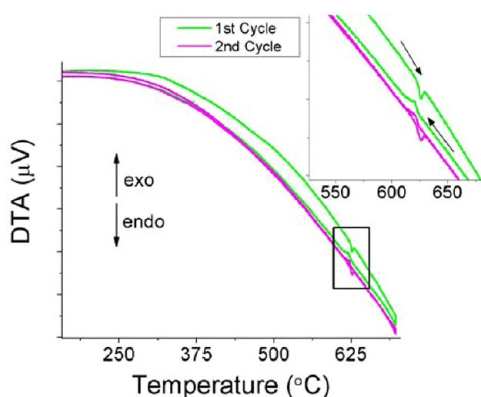

Figure 5. Differential thermal analysis on single crystals of O-CePd$_{3.21}$Ga$_{7.79}$. An endothermic (heating) and exothermic (cooling) peak at ~620 °C corresponds to the phase transition to the cubic phase. The transition is reversible as observed over two heating cycles.

transition, observed over two heating and cooling cycles, is apparent at ~620 °C. To probe this transition in more detail, a powdered sample was analyzed at the Advanced Photon Source by high resolution powder diffraction on beamline 11-BM. During heating to 675 °C, *in situ* measurements uncovered complex atom movement within the cell before and after the main transition to higher symmetry. Powder diffraction

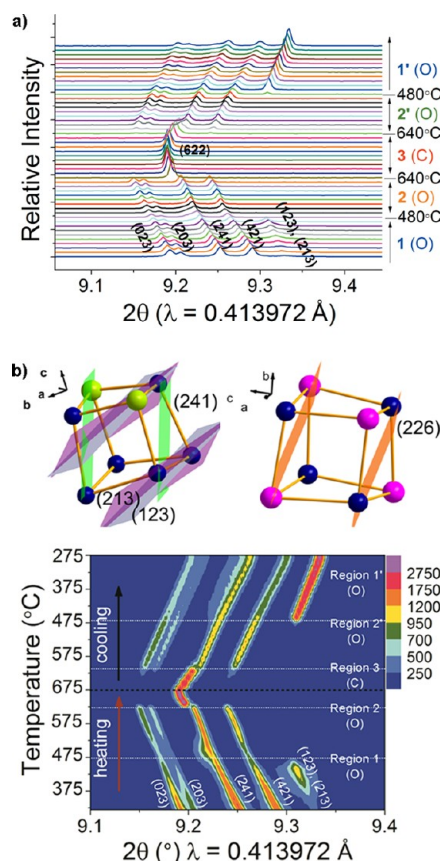patterns, collected every 3 min while heating and cooling continuously, are shown in Figure 6a.

Figure 6. *In situ* temperature-dependent high resolution PXRD of O-CePd$_{3.21}$Ga$_{7.79}$ collected on 11-BM at APS. (a) All scans collected during one heating and cooling cycle from 300 to 675 °C. Three distinct regions exist, labeled 1−3. A clear transition to higher symmetry occurs above ~640 °C (region 3). (b) Contour map of zoomed region from 9.1°< 2Θ < 9.4°. The intensities of the (123) and (213) reflections grow in region 1 on heating and then disappear as the temperature enters region 2. The (123), (213), and (241) planes are drawn over the cubic unit of the orthorhombic cell and compared to the cubic cell.

Three distinct regions are visible upon heating from 300 to 675 °C (Figure 6a): (1) a slow transition up to ~480 °C in which several Bragg peaks increase in intensity and others broaden, (2) a reorganized orthorhombic phase that exists in the temperature range ~480 to 640 °C and (3) a quick transition to C-CePd$_{2.69}$Ga$_{8.31}$ above 640 °C. The reverse process occurs on cooling, denoted by regions 1′, 2′, and 3′ in Figure 7a,b. The variable temperature PXRD is expanded in Figure 6b in the range of 9.1 < 2Θ < −9.4° to illustrate these unique temperature ranges. Region 1 shows the gradual growth of orthorhombic (123) and (213) reflections, which implies increased electron density within these planes. At the same time, the orthorhombic (241) reflection decreases in intensity up to the transition into region 2, When the temperature reaches ~480 °C, the (123) and (213) reflections quickly vanish, perhaps caused by a transition to higher symmetry and/or new reflection conditions. The remaining reflections, including the former (241) reflection, of the rearranged phase regain intensity and stay constant through the nearly 200 °C span of region 2. The major phase transition occurs around 640
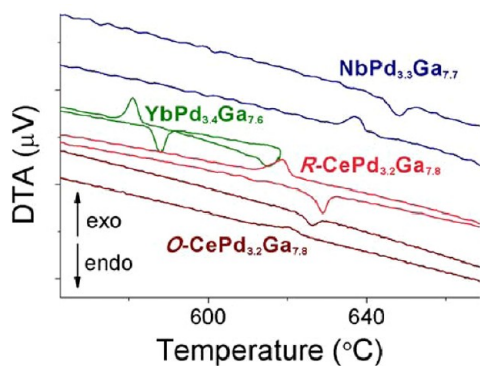
Figure 7. Differential thermal analyses on single crystals of NdPd$_{3+x}$Ga$_{8-x}$ and YbPd$_{3+x}$Ga$_{8-x}$ (blue and green, respectively) show similar transitions to *O*- and *R*-CePd$_{3+x}$Ga$_{8-x}$ (green) around 600 °C.

°C in which the powder pattern simplifies to the high symmetry cubic phase in region 3. Figure 6b shows these reflection planes drawn over the cubic structural units of *O*-CePd$_{3.21}$Ga$_{7.79}$ and *C*-CePd$_{2.69}$Ga$_{8.31}$. The differences in elemental site occupancies and bonding pairs necessarily imply a displacive phase transition[45] that proceeds through a closely related intermediate phase (region 2). This is clearly evident in the structure of the annealed *Pm$\overline{3}$m* CePd$_{2.9(1)}$Ga$_{8.1(1)}$ (Table 2), which has not completely converted to *Fm$\overline{3}$m* symmetry. Both positional and elemental disorder are evident in the cubic structural unit. Given the smaller Pd:Ga ratio in the cubic phase, parts of the sample presumably decompose into Ce–Pd species and, therefore, the transition is likely to become irreversible after a number of cycles. Increased surface roughness was observed on single crystals after cycling twice during the transition and supports slight degradation.

On heating, the temperature range for coexistence of *O*- and *C*-CePd$_{3+x}$Ga$_{8-x}$ phases is very narrow; the cubic (622) reflection is not clearly visible by eye below 640 °C and the same applies to orthorhombic reflections above 640 °C. On cooling, the coexistence range looks to be greater as growth of the orthorhombic (241) reflection and decrease of the cubic reflections is detectable in several patterns through the phase transition. Similar behavior through regions 1 and 2 is observed for several reflections at other 2Θ angles. Considering the extent of atomic displacements that must occur, it is fascinating that the crystal lattice remains intact throughout the phase transition. The smaller energy barrier to an intermediate phase must play a key part in aiding the high temperature transition to the cubic phase.

Rare Earth Analogues REPd$_{3+x}$Ga$_{8-x}$. Syntheses in Ga flux were successful in producing REPd$_{3+x}$Ga$_{8-x}$ for RE = La, Nd, Sm, Tm, Yb. The cell parameters for the analogue

compounds are given in Table 4. Cooling rate experiments were not performed for the analogues as was done for the Ce compounds; however, all analogues formed as one of the lower symmetry forms, *R$\overline{3}$m* or *Pmmn*. Differential thermal analysis on the Nd and Yb analogues also show phase transitions above 600 °C (Figure 7). DTA was performed on the Tm analogue, but no phase transitions were observed up to 800 °C.

A plot of cell volume vs rare earth ionic radius,[46,47] Figure 8, shows a positive deviation from Vegard's law for the Yb
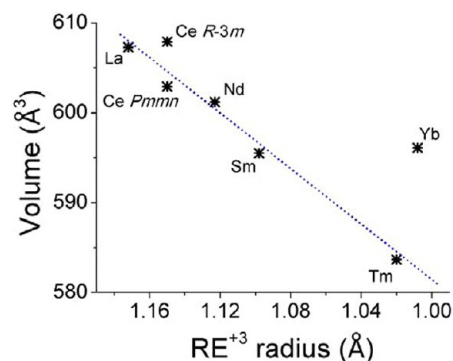

Figure 8. Unit cell volume (normalized to a 8 × 8 × 8 Å cell) vs rare earth radius for REPd$_{3+x}$Ga$_{8-x}$ analogues.

analogue, which indicates mixed or Yb^{2+} valence. Magnetic susceptibility data for *R*-YbPd$_{3+x}$Ga$_{8-x}$ (not shown) supports this conclusion with temperature-independent Pauli paramagnetic behavior down to 2 K. Interestingly, the Yb phase was isolated in a previous study via a direct combination melt reaction and crystallized in the cubic *Pm$\overline{3}$m* space group.[23] This difference emphasizes how use of the molten metal flux technique can widen our capabilities for finding new compounds and also new structural variants of compounds. In solution, compounds that initially form at high temperature remain reactive, with bonds constantly breaking and reforming in ways inaccessible through fast direct combination melting techniques.

Instabilities have proven to be prevalent in many BaHg$_{11}$-type compounds. The family of BaHg$_{11}$-type aluminides R$_3$Au$_{6+x}$Al$_{26}$T (R = Ca, Sr, Eu, Yb; T = early transition metal) show several modifications to the parent structure in order to retain stability.[29] These modifications include split atomic positions in the crystals structure, mixed metal sites, and, for all synthesized aluminides, a stuffed Au atom in the cubic structural unit. More than 40 aluminides with the BaHg$_{11}$ structure type were analyzed, and an interesting correlation was found between stability and cell volume. Below a cell volume of 630 Å^3, a structural model could not satisfactorily be refined from single crystal X-ray diffraction data. It is possible that

Table 4. Cell Parameters and Synthesis Details for Rare Earth Analogues of REPd$_{3+x}$Ga$_{8-x}$ (RE = La, Nd, Sm, Tm, Yb)

RE analogue	space group	cell parameters					crystal Pd:Ga ratio	reaction temp (°C)	final temp (°C)	cool rate (°C/h)
		a (Å)	*b* (Å)	*c* (Å)	*α* (deg)	volume (Å^3)				
LaPd$_{2.9}$Ga$_{8.1}$	*R-3m*	8.4590(9)	8.4590(9)	8.4590(9)	90.069(8)	607.43(11)	0.36	950	300	12
NdPd$_{3.3}$Ga$_{7.7}$	*Pmmn*	11.8808(9)	11.9282(8)	8.4850(6)	90	1202.46(15)	0.43	860	300	27
SmPd$_{3.0}$Ga$_{8.0}$	*R-3m*	8.4131(8)	8.4131(8)	8.4131(8)	89.960(7)	595.49(9)	0.38	860	300	23
TmPd$_{2.88}$Ga$_{8.12}$	*R-3m*	8.3571(7)	8.3571(7)	8.3571(7)	89.999(7)	583.65(8)	0.35	860	300	23
YbPd$_{3.4}$Ga$_{7.6}$	*R-3m*	8.4162(8)	8.4162(8)	8.4162(8)	90.116(7)	596.14(10)	0.45	860	400	10

these systems, which were grown from aluminum flux, have lost cubic symmetry and have been stabilized in a lower symmetry space group, with rhombohedral or orthorhombic symmetry as observed in the $REPd_{3+x}Ga_{8-x}$ analogues. Given that C-$CePd_{2.69}Ga_{8.31}$ is stable only at high temperature, cell contraction upon cooling could be the predominant driving force for the phase transition to lower symmetry in $REPd_{3+x}Ga_{8-x}$ as cell contraction through chemical substitution causes instability in the aluminides. This may also explain why R-$TmPd_{2.88}Ga_{8.12}$ does not convert to cubic symmetry below 800 °C, as it has the smallest cell volume among the Pd analogues and may require much greater temperatures to expand and stabilize a cubic structure.

Physical Properties. The long Ce–Ce distances (~6 Å) in $CePd_{3+x}Ga_{8-x}$ imply that magnetic interactions, if present, occur indirectly through a Ruderman–Kittel–Kasuya–Yosida (RKKY) mechanism,[48–50] in which exchange interactions are facilitated by conduction electrons. We used magnetic susceptibility measurements, as well as heat capacity and electrical resistivity, to learn about the interactions in the $CePd_{3+x}Ga_{8-x}$ system.

Magnetic Susceptibility. Zero field-cooled (ZFC) and field-cooled (FC) magnetic susceptibility versus temperature plots of single crystals of O-$CePd_{3.21}Ga_{7.79}$, collected on warming under an applied field of 10 kOe, are shown in Figure 9 plotted against previously reported magnetic
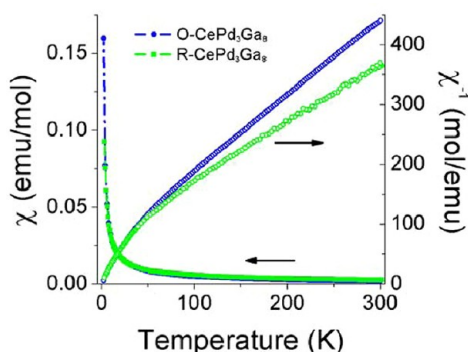
Figure 9. Temperature-dependent magnetic susceptibility of O-$CePd_{3.21}Ga_{7.79}$ and R-$CePd_3Ga_8$[41] under 10 kOe applied field. The inverse susceptibility is linear with temperature above 50 K. A fit of the O-$CePd_{3.21}Ga_{7.79}$ field-cooled susceptibility data to a modified Curie–Weiss law (with temperature independent parameter, χ_0) gives $C = 0.720(3)$ emu/(mol K^2), $\Theta = -39.6(4)$ K, $\chi_0 = 1.45(7) \times 10^{-4}$ emu/mol.

susceptibility on R-$CePd_3Ga_8$.[41] The inverse susceptibility data follow a modified Curie–Weiss law down to ~50 K: $\chi(T) = C/(T - \Theta) + \chi_0$, where C is the Curie constant, Θ is the Weiss temperature, and χ_0 is a temperature-independent paramagnetic term associated with the conduction electrons of the metallic compound. Directly fitting the paramagnetic region of the data (80–300 K) to the nonlinear Curie–Weiss law gives parameters $C = 0.720(3)$ (emu K)/mol, $\Theta = -39.6(4)$ K, $\chi_0 = 1.45(7) \times 10^{-4}$ emu/mol. The calculated effective moment of $2.400(8)\mu_B$ is slightly lower than the theoretical moment for free trivalent Ce ions ($2.54\ \mu_B/Ce^{3+}$);[51] this suppression could be due to quenching from spin–orbit coupling or crystal field interactions.[52] The transition metal, Pd, does not carry a significant magnetic moment, as was also found for R-$CePd_{3.13}Ga_{7.87}$.

Magnetic susceptibilities of R-$CePd_{3.13}Ga_{7.87}$ and O-$CePd_{3.21}Ga_{7.79}$ were also measured under low applied field (<100 Oe) and temperatures down to <1.5 K. Plots are shown in Figure 10a and Figure 10b. The transition seen in Figure 10a,
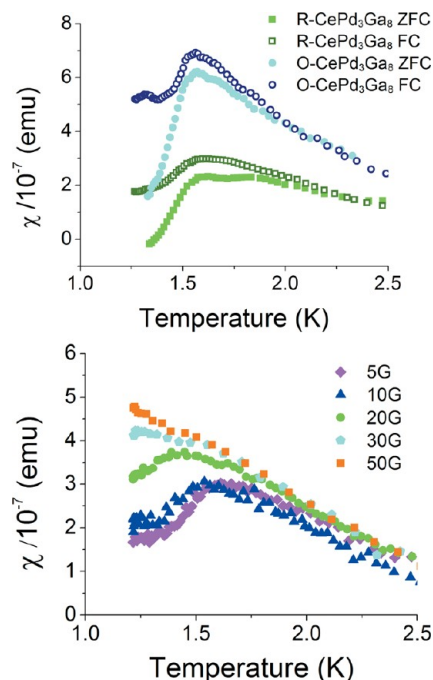
Figure 10. Low field magnetic susceptibility measurements on single crystals of $CePd_{3+x}Ga_{8-x}$. (Top) Magnetic susceptibility vs temperature on both O- (blue) and R- (green) $CePd_{3+x}Ga_{8-x}$ under 5 G. The maximum peak and divergence of field-cooled and zero field-cooled data are indicative of antiferromagnetic ordering. (Bottom) Magnetization vs temperature plots on the rhombohedral phase under gradually increasing applied field plots. The magnetic interactions are essentially quenched at 50 G.

around 1.65 K, is characteristic of an antiferromagnetic transition. Both R-$CePd_{3.13}Ga_{7.87}$ and O-$CePd_{3.21}Ga_{7.79}$ showed similar low temperature behavior. Field-dependent susceptibility plots in Figure 10b show the gradual suppression of the transition in increasing applied field. The weak correlations are almost completely quenched under an applied field of 50 Oe.

For magnetic structures, one can expect the ordering temperature to coincide approximately with the paramagnetic Weiss temperature, giving a ratio $|\Theta|/T_C$ close to 1.[53,54] For antiferromagnetic interactions ($T_C = T_N$), this ratio can deviate slightly. Examples include Eu_2AuGe_3 ($|\Theta|/T_N = 0.73$),[7] $PrIr_2Ge_2$ ($|\Theta|/T_N = 2.3$),[55] and $CeRuSn$ ($|\Theta|/T_N = 3.7$).[56] In magnetically frustrated systems, a large deviation between Θ and T_N is observed as the spins cannot order despite strong exchange interactions. In these cases, the ratio $|\Theta|/T_N$ can be called a frustration factor, f, and helps describe the degree of frustration in different compounds.[53,57]

The large Weiss temperature for $CePd_{3+x}Ga_{8-x}$, −39.6 K, suggests a much higher ordering temperature than the $T_N = 1.65$ K ordering temperature observed in low field magnetic susceptibility data. The contrasting temperatures give a frustration factor of $f = 24$. The degree of frustration is three times greater than that found in the intermetallic $Ce_5Ni_2Si_3$, with $f = 8.4$[58] and almost double that of Li_7RuO_6 ($f = 12.5$).[59] In addition, the broad maximum and bifurcation of ZFC and FC plots in the temperature-dependent susceptibility data may

be indications of fluctuating short-range interactions, which can arise from magnetic frustration.[60−62] Further studies are needed to determine the origins of the anomalous Néel temperature.

Electrical Transport Properties. The electrical resistivity of O-$CePd_{3.21}Ga_{7.79}$ is plotted down to 1.5 K in Figure 11 and
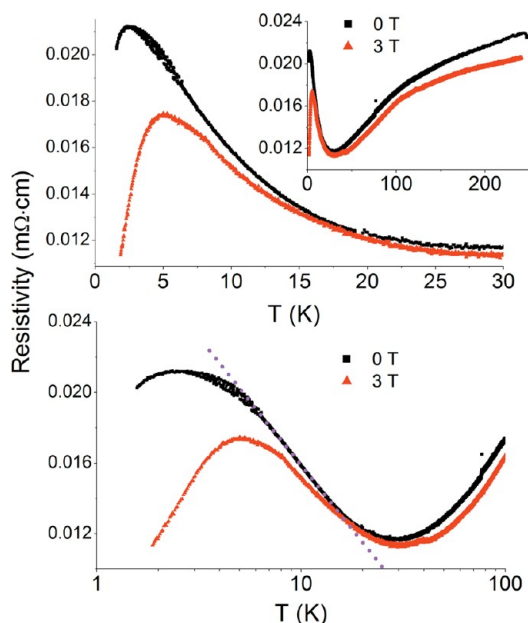

Figure 11. Single crystal electrical resistivity of O-$CePd_{3.21}Ga_{7.79}$ under applied fields of zero and 3 T. Inset shows the full temperature range from 1.5 to 250 K (3 T applied field). Bottom graph shows resistivity versus log T to show the Kondo-like linear region between the minimum and peak maximum (dashed line is drawn over 0 T applied field data to emphasize linear region).

shows a broad peak centered around 2 K. The resistivity features a negative curvature around 150 K and finds a minimum value around 30 K before rapidly increasing with decreasing temperature. This behavior is characteristic of Kondo systems,[63−65] as was determined for R-$CePd_3Ga_8$.[41] Similar temperature dependence is observed in the geometrically frustrated Kondo antiferromagnetic, CePdAl, as well.[66] The region just below the minimum, 2 K < T < 30 K, shows a linear ρ vs $-\log T$ relationship, which is consistent with the Kondo effect, where at low temperatures the conduction electrons are scattered from the local magnetic moments of the Ce atoms.[67] A downturn in resistivity associated with antiferromagnetic correlations is observed below 2 K.

The total specific heat of R-, O-, and C-$CePd_{3+x}Ga_{8−x}$, from 2 to 20 K, is plotted in Figure 12. A large λ-type peak, which is expected for antiferromagnetic transitions, is observed at T_N around 1.6 K. The peak position varies between each phase, which can be attributed to the difference in structures. Multiple peaks are visible in O-$CePd_{3.21}Ga_{7.79}$ and most likely indicate an inclusion of rhombohedral and cubic phases. A second, smaller peak is observed in all phases as well. For R- and O-$CePd_{3+x}Ga_{8−x}$, the peak is positioned just above 2 K while for C-$CePd_{3+x}Ga_{8−x}$ it lies below the antiferromagnetic peak. Field-dependent measurements were performed on R-$CePd_{3+x}Ga_{8−x}$ to probe the transitions further (Figure 13). Under an applied field of 30 kOe, as expected for antiferromagnetic correlations, the low temperature peak shifts to lower temperature and decreases in intensity until it is no longer visible at an applied field of 90 kOe. The second peak increases in intensity and
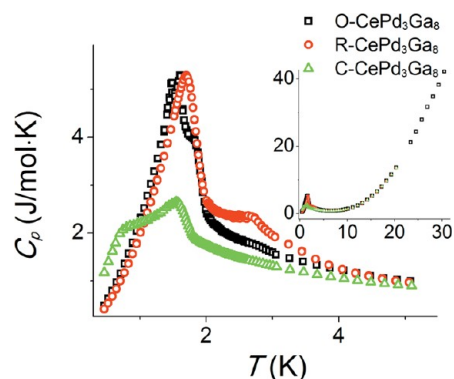

Figure 12. Total specific heat of O- (black squares), R- (red circles), and C-$CePd_{3+x}Ga_{8−x}$ (green triangles) compounds. The large peaks are associated with the antiferromagnetic transition while the smaller peaks may be due to Kondo, crystal electric field, and frustration effects.
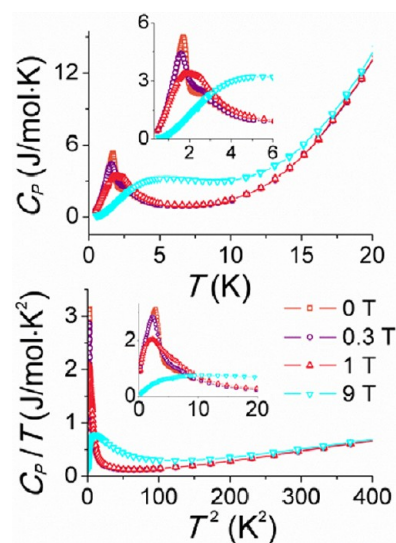

Figure 13. Specific heat of O-$CePd_{3.21}Ga7.79$ under 0, 0.3, 1, and 9 T applied field. Top: C_P vs T shows two peaks below 10 K that are sensitive to applied field. Bottom: C_P/T vs T^2. Zoomed-in views are shown as insets.

broadens with increasing field and shifts to higher temperature. This behavior is consistent with increased splitting of low-lying energy states and possibly originates from both Kondo and crystal electrical field effects, common in heavy fermion intermetallic compounds, as observed, for example, in CePdAl,[66] $Yb_2(Pd_{1−x}Ni_x)_2Sn$,[68] and $CeNiGe_3$.[69] More effective probes, such as neutron scattering experiments, would help clarify the nature of the ground-state electronic structure.

The specific heat of R-$YbPd_{3+x}Ga_{8−x}$ was also measured at low temperature, shown in Figure 14. In contrast to the $CePd_{3+x}Ga_{8−x}$ phases, no low temperature peaks were observed for the Yb analogue. A positive curvature in C_p/T vs T^2 is observed below 1.5 K. A linear fit of the data in the temperature regions both above and below the minimum gives a γ value on the order of only 10 mJ/(mol K^2); therefore, R-$YbPd_{3+x}Ga_{8−x}$ is not considered a heavy fermion compound.

■ **CONCLUSIONS**

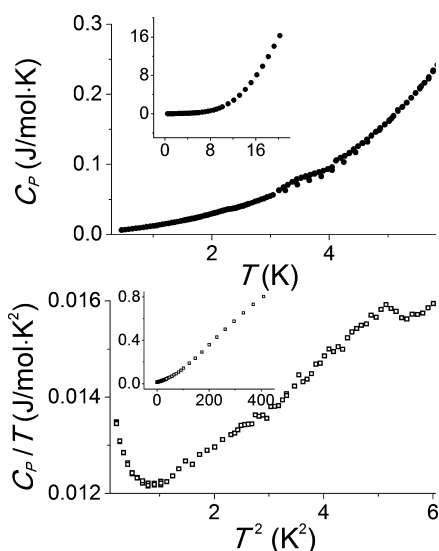Three forms of $CePd_{3+x}Ga_{8−x}$ have been isolated from reactions in molten Ga with molar ratio 1Ce:4Pd:15Ga. The compound

Figure 14. Specific heat of R-YbPd$_{3+x}$Ga$_{8-x}$. Top: C_p vs T shows no anomalies at low temperature. Bottom: C_p/T vs T^2 shows positive curvature below 1.5 K, but the phase is not considered a heavy fermion compound. Insets show the full temperature range.

first forms as a $Fm\bar{3}m$ cubic structure, which can be quenched out of solution at 675 °C. If the reaction is allowed to cool to lower temperatures, the cubic phase transforms to two lower symmetry forms, which can be selectively favored one over the other by varying the cooling rate. An orthorhombic $Pmmn$ cell results for slow cooling rates down to 600 °C, and rhombohedral $R\bar{3}m$ results for a faster cooling rate down to 300 °C. This transformation between cubic and low symmetry forms also occurs out of solution, as evidenced by differential thermal analysis and combined annealing and single crystal X-ray diffraction experiments. *In situ* variable temperature and high resolution powder X-ray diffraction experiments on orthorhombic CePd$_{3.21}$Ga$_{7.79}$ show an initial rearrangement of atoms about select lattice planes and conversion to an intermediate phase approximately 200 °C before the transformation to the cubic phase.

The rare earth analogue series REPd$_{3+x}$Ga$_{8-x}$ (RE = La, Nd, Sm, Tm, Yb) also form in Ga flux. As with Ce, only low symmetry orthorhombic or rhombohedral phases were isolated below 400 °C. Differential thermal analysis on the Nd and Yb analogues also showed a phase transition above 600 °C, but a transition was not detected in R-TmPd$_{2.88}$Ga$_{8.12}$. This may be due to the stability offered by a smaller rare earth element.

Anomalously weak antiferromagnetic ordering in both O-CePd$_{3.21}$Ga$_{7.79}$ and R-CePd$_{3.13}$Ga$_{7.87}$ at T_N = 1.65 K is indicative of magnetic suppression, possibly frustration. Specific heat and electrical resistivity measurements exhibit characteristics of the Kondo effect. Additional studies, such as inelastic neutron scattering techniques, would help to interpret the low temperature phenomena as well as illuminate the magnetic structures of these new phases.

ASSOCIATED CONTENT

⑤ Supporting Information

Atomic positions and anisotropic atomic displacement parameters for CePd$_{3+x}$Ga$_{8-x}$ compounds. High resolution powder X-ray diffraction refinement. This information is available free of charge via the Internet at http://pubs.acs.org/.

AUTHOR INFORMATION

Corresponding Author

m-kanatzidis@northwestern.edu

Notes

The authors declare no competing financial interest.

REFERENCES

(1) Phelan, W. A.; Menard, M. C.; Kangas, M. J.; McCandless, G. T.; Drake, B. L.; Chan, J. L. Y. *Chem. Mater.* **2012**, *24*, 409.

(2) Kanatzidis, M. G.; Pottgen, R.; Jeitschko, W. *Angew. Chem., Int. Ed.* **2005**, *44*, 6996.

(3) Li, B.; Kim, S. J.; Miller, G. J.; Corbett, J. D. *Inorg. Chem.* **2010**, *49*, 1503.

(4) Maple, M. B.; Baumbach, R. E.; Hamlin, J. J.; Zocco, D. A.; Taylor, B. J.; Butch, N. P.; Jeffries, J. R.; Weir, S. T.; Sales, B. C.; Mandrus, D.; McGuire, M. A.; Sefat, A. S.; Jin, R.; Vohra, Y. K.; Chu, J. H.; Fisher, I. R. *Phys. B* **2009**, *404*, 2924.

(5) Berthebaud, D.; Goncalves, A. P.; Tougait, O.; Potel, M.; Lopes, E. B.; Noel, H. *Chem. Mater.* **2007**, *19*, 3441.

(6) Kim, S. J.; Kraus, F.; Fassler, T. F. *J. Am. Chem. Soc.* **2009**, *131*, 1469.

(7) Sebastian, C. P.; Malliakas, C. D.; Chondroudi, M.; Schellenberg, I.; Rayaprol, S.; Hoffmann, R. D.; Pottgen, R.; Kanatzidis, M. G. *Inorg. Chem.* **2010**, *49*, 9574.

(8) Chondroudi, M.; Balasubramanian, M.; Welp, U.; Kwok, W. K.; Kanatzidis, M. G. *Chem. Mater.* **2007**, *19*, 4769.

(9) Bobev, S.; Hullmann, J.; Harmening, T.; Pottgen, R. *Dalton Trans.* **2010**, *39*, 6049.

(10) Stojanovic, M.; Latturner, S. E. *J. Solid State Chem.* **2007**, *180*, 907.

(11) Canfield, P. C.; Fisk, Z. *Philos. Mag. B* **1992**, *65*, 1117.

(12) Salvador, J. R.; Gour, J. R.; Bilc, D.; Mahanti, S. D.; Kanatzidis, M. G. *Inorg. Chem.* **2004**, *43*, 1403.

(13) Thomas, E. L.; Millican, J. N.; Okudzeto, E. K.; Chan, J. Y. *Comments Inorg. Chem.* **2006**, *27*, 1.

(14) Menard, M. C.; Drake, B. L.; McCandless, G. T.; Thomas, K. R.; Hembree, R. D.; Haldolaarachchige, N.; DiTusa, J. F.; Young, D. P.; Chan, J. Y. *Eur. J. Inorg. Chem.* **2011**, 3909.

(15) (a) Macaluso, R. T.; Millican, J. N.; Nakatsuji, S.; Lee, H.-O.; Carter, B.; Moreno, N. O.; Fisk, Z.; Chan, J. Y. *J. Solid State Chem.* **2005**, *178*, 3547. (b) Chen, X. Z.; Small, P.; Sportouch, S.; Zhuravleva, M. A.; Brazis, P.; Kannewurf, C. R.; Kanatzidis, M. G. *Chem. Mater.* **2000**, *12*, 2520. (c) Zhuravleva, M. A.; Kanatzidis, M. G. *J. Solid State Chem.* **2003**, *173*, 280. (d) Zhuravleva, M. A.; Wang, X. P.; Schultz, A. J.; Bakas, T.; Kanatzidis, M. G. *Inorg. Chem.* **2002**, *41*, 6056.

(16) Macaluso, R. T.; Nakatsuji, S.; Lee, H.; Fisk, Z.; Moldovan, M.; Young, D. P.; Chan, J. Y. *J. Solid State Chem.* **2003**, *174*, 296.

(17) Kim, J. W.; Kwon, Y. S. *Phys. B* **2006**, *378−380*, 833.

(18) Li, D. X.; Nimori, S.; Kitazawa, H.; Shiokawa, Y. *Phys. B* **2006**, *378−380*, 805.

13008

dx.doi.org/10.1021/ja302812s | *J. Am. Chem. Soc.* 2012, 134, 12998−13009

(19) Keller, L.; Donni, A.; Kitazawa, H.; van den Brandt, B. *Appl. Phys. A* **2002**, *74*, S686.

(20) Donni, A.; Ehlers, G.; Maletta, H.; Fischer, P.; Kitazawa, H.; Zolliker, M. *J. Phys.-Condens. Matter* **1996**, *8*, 11213.

(21) Peyronel, G. *Gazz. Chim. Ital.* **1952**, *82*, 679.

(22) Gladyshevskii, R. E.; Cenzual, K. *J. Alloys Compd.* **1996**, *240*, 266.

(23) Grin, Y. N.; Hiebl, K.; Rogl, P.; Godart, C.; Alleno, E. *J. Alloys Compd.* **1997**, *252*, 88.

(24) Biehl, E.; Deiseroth, H. J. *Z. Anorg. Allg. Chem.* **1999**, *625*, 1073.

(25) Latturner, S. E.; Kanatzidis, M. G. *Inorg. Chem.* **2004**, *43*, 2.

(26) Fedyna, L. O.; Bodak, O. I.; Fedorchuk, A. O.; Tokaychuk, Y. O. *J. Solid State Chem.* **2005**, *178*, 1874.

(27) Gumeniuk, R. V.; Akselrud, L. G.; Stel'makhovych, B. M.; Kuz'ma, Y. B. *J. Alloys Compd.* **2005**, *389*, 127.

(28) Li, B.; Corbett, J. D. *Inorg. Chem.* **2006**, *45*, 3861.

(29) Latturner, S. E.; Bilc, D.; Mahanti, S. D.; Kanatzidis, M. G. *Inorg. Chem.* **2009**, *48*, 1346.

(30) Stelmakhovych, O.; Stelmakhovych, B.; Kalychak, Y.; Havela, L. *Intermetallics* **2010**, *18*, 569.

(31) Verbovytskyy, Y.; Goncalves, A. P. *Intermetallics* **2010**, *18*, 655.

(32) Wang, F.; Pearson, K. N.; Straszheim, W. E.; Miller, G. L. *Chem. Mater.* **2010**, *22*, 1798.

(33) Verbovytskyy, Y.; Pereira, L. C. J.; Goncalves, A. P. *J. Alloys Compd.* **2011**, *509*, L14.

(34) Yoshiuchi, S.; Takeuchi, T.; Ohya, M.; Katayama, K.; Matsushita, M.; Yoshitani, N.; Nishimura, N.; Ota, H.; Tateiwa, N.; Yamamoto, E.; Haga, Y.; Yamagami, H.; Honda, F.; Settai, R.; nuki, Y. *J. Phys. Soc. Jpn.* **2010**, *79*, 044601.

(35) *X-AREA*, version 1.39; STOE & Cie GmbH: Darmstadt, Germany, 2006.

(36) Sheldrick, G. M. *SHELXTL Structure Determination Programs*, version 6.14; . Bruker AXS Inc.: Madison, WI, 2000−2003.

(37) Toby, B. H.; Huang, Y.; Dohan, D.; Carroll, D.; Jiao, X.; Ribaud, L.; Doebbler, J. A.; Suchomel, M. R.; Wang, J.; Preissner, C.; Kline, D.; Mooney, T. M. *J. Appl. Crystallogr.* **2009**, *42*, 990.

(38) Wang, J.; Toby, B. H.; Lee, P. L.; Ribaud, L.; Antao, S. M.; Kurtz, C.; Ramanathan, M.; Von Dreele, R. B.; Beno, M. A. *Rev. Sci. Instrum.* **2008**, *79*.

(39) Bain, G. A.; Berry, J. F. *J. Chem. Educ.* **2008**, *85*, 532.

(40) Vandervoort, K. G.; Griffith, G.; Claus, H.; Crabtree, G. W. *Rev. Sci. Instrum.* **1991**, *62*, 2271.

(41) Macaluso, R. T.; M., F.; Young, D. P.; Stadler, S.; Mitchell, J. F.; Geiser, U.; Hong, H. Y.; Kanatzidis, M. G. *J. Solid State Chem.* **2011**, *184*, 3185.

(42) Higashi, I.; Kitazawa, H.; Kobayashi, K.; Yoshida, M.; Sato, N.; Komatsubara, T. *J. Alloys Compd.* **1993**, *191*, L21.

(43) Hulliger, F. *J. Alloys Compd.* **1993**, *196*, 225.

(44) Xue, B.; Schwer, H.; Hulliger, F. *Acta Crystallogr. Sect. C: Cryst. Struct. Commun.* **1994**, *50*, 338.

(45) Christy, A. *Acta Crystallogr. Sect. B* **1993**, *49*, 987.

(46) Jia, Y. Q. *J. Solid State Chem.* **1991**, *95*, 184.

(47) Shannon, R. *Acta Crystallogr., Sect. A* **1976**, *32*, 751.

(48) Yosida, K. *Phys. Rev.* **1957**, *106*, 893.

(49) Kasuya, T. *Prog. Theor. Phys.* **1956**, *16*, 45.

(50) Ruderman, M. A.; Kittel, C. *Phys. Rev.* **1954**, *96*, 99.

(51) Lock, J. *Component Parts, IRE Trans.* **1959**, *6*, 93.

(52) Richter, M. *J. Phys. D: Appl. Phys.* **1998**, *31*, 1017.

(53) Greedan, J. E. *J. Mater. Chem.* **2001**, *11*, 37.

(54) Ramirez, A. P. *Annu. Rev. Mater. Sci.* **1994**, *24*, 453.

(55) Anand, V. K.; Hossain, Z.; Ramakrishnan, S. *J. Alloys Compd.* **2011**, *509*, 1436.

(56) Mydosh, J. A.; Strydom, A. M.; Baenitz, M.; Chevalier, B.; Hermes, W.; Pottgen, R. *Phys. Rev. B* **2011**, *83*, 054411.

(57) Schiffer, P.; Ramirez, A. P. *Comments Condens. Matter Phys.* **1996**, *18*, 21.

(58) Lee, B. K.; Ryu, D. H.; Kim, D. Y.; Hong, J. B.; Jung, M. H.; Kitazawa, H.; Suzuki, O.; Kimura, S.; Kwon, Y. S. *Phys. Rev. B* **2004**, *70*.

(59) Kitazawa, H.; Schank, C.; Thies, S.; Seidel, B.; Geibel, C.; Steglich, F. *J. Phys. Soc. Jpn.* **1992**, *61*, 1461.

(60) Kim, M. S.; Bennett, M. C.; Aronson, M. C. *Phys. B* **2008**, *403*, 1411.

(61) Singh, S.; Saha, S.; Dhar, S. K.; Suryanarayanan, R.; Sood, A. K.; Revcolevschi, A. *Phys. Rev. B* **2008**, *77*.

(62) Li, D.; Nimori, S.; Kitazawa, H.; Shiokawa, Y. *Phys. B* **2006**, *378−80*, 805.

(63) Anand, V. K.; Adroja, D. T.; Hillier, A. D.; Kockelmann, W.; Fraile, A.; Strydom, A. M. *J. Phys.-Condens. Matter* **2011**, *23*.

(64) Pasturel, M.; Tougait, O.; Potel, M.; Roisnel, T.; Wochowski, K.; Noel, H.; Troc, R. *J. Phys.-Condens. Matter* **2009**, *21*.

(65) Kaczorowski, D.; Andraka, B.; Zaremba, V. I.; Marucha, C. *Phys. B* **2000**, *281*, 44.

(66) Kitazawa, H.; Matsushita, A.; Matsumoto, T.; Suzuki, T. *Phys. B* **1994**, *199*, 28.

(67) Avila, M. A.; Sera, M.; Takabatake, T. *Phys. Rev. B* **2004**, *70*, 100409.

(68) Kikuchi, F.; Hara, K.; Matsuoka, E.; Onodera, H.; Nakamura, S.; Nojima, T.; Katoh, K.; Ochiai, A. *J. Phys. Soc. Jpn.* **2009**, *78*, 083708.

(69) Mun, E. D.; Bud'ko, S. L.; Kreyssig, A.; Canfield, P. C. *Phys. Rev. B* **2010**, *82*, 054424.